UAV Thermography for Building Energy Audit: Comparing Image Acquisition Strategies

Cheng Zhang[a], Yang Zou[a], Johannes Dimyadi[b,c] and Vicente Gonzalez[d]

[a]Department of Civil and Environmental Engineering, University of Auckland, Auckland 1010, New Zealand
[b]School of Computer Science, University of Auckland, Auckland 1010, New Zealand
[c]Codify Asset Solutions Limited (CAS), Auckland 1010, New Zealand
[d]Department of Civil and Environmental Engineering, University of Alberta, Edmonton, Canada
czha626@aucklanduni.ac.nz, yang.zou@auckland.ac.nz, jdimyadi@cas.net.nz, vagonzal@ualberta.ca

Abstract –

Maintaining energy performance of ageing building stock has become a global priority towards a more environmentally sustainable future in the age of climate change. Unmanned Aerial Vehicle (UAV) equipped with thermal camera is increasingly used for building inspection. However, scant attention has been paid to the satisfactory image acquisition strategy for a rigorous building energy audit. To narrow this research gap, this paper undertakes a comparative analysis of the impact of three primary features of UAV thermal image collection strategies on accurate thermal anomaly evaluation. Firstly, a laboratory-scale building featuring artificial thermal anomalies was developed and constructed. Then, UAV thermal images were collected under various inspection conditions, examining features including (1) temperature difference between interior and exterior environments, (2) ground sampling distance (GSD), and (3) UAV oblique angle. GSD herein refers to the GSD of the collected UAV thermal images. The collected thermal images underwent a comprehensive analysis and comparison to understand the influence of the three features. The results suggest that: (1) thermal images collected with highest interior and exterior temperature difference are recommended for identifying all potential thermal anomalies; (2) a GSD of within $5\,mm$ is recommended to ensure the visibility of thermal damages in the collected thermal images; (3) a multi-scale thermal image collection strategy is recommended for an efficient and accurate evaluation of thermal anomalies, especially minor defects; (4) a UAV oblique angle within 30° is recommended to ensure a high image contrast between damaged and undamaged areas on the inspected façade.

Keywords –

Building energy audit; Unmanned aerial vehicle (UAV); Aerial thermography; Image acquisition strategy

1 Introduction

Reducing energy consumption and greenhouse gas emission has become a global priority in the age of climate change. The built environment currently accounts for around 30% of global final energy consumption and over 33% of global energy- and process-related CO_2 emission [1]. Maintaining the energy performance of ageing buildings is crucial towards an environmentally sensitive and sustainable future. In recent years, considerable research efforts have been made to understand the building façade energy performance and conduct timely maintenance.

Thermal anomalies in building façades, such as heat loss and insulation failure, are the primary reasons for poor energy performance [2]. One commonly used method to diagnose these thermal anomalies is infrared thermography (IRT), which captures thermal images representing surface temperatures [3]. IRT has been widely used for building energy audits, considering its non-invasive nature [4]. Thermal anomalies generally feature significant variations in the surface temperatures, which are easily identifiable in thermal images [5]. However, traditional terrestrial or hand-held IRT requires inspectors to physically visit the site, which is time-consuming, labour-intensive, and subject to safety risks, especially when it comes to hard-to-reach areas, such as high-rise buildings.

With the rapid evolution and use of Unmanned Aerial Vehicle (UAV) technology, aerial thermography has become a safe, cost-efficient, and fast solution for collecting close-range thermal images of building façades [6]. Thermal anomalies, such as thermal bridges, heat loss, and insulation failure, can be automatically extracted from UAV-collected thermal images through digital image processing [7] and deep learning [8] algorithms. Additionally, a 3D thermal model can be generated to facilitate a comprehensive understanding of the building energy performance [9].

A key factor in achieving successful UAV thermography for building energy audits is the implementation of a suitable image acquisition strategy, i.e., UAV flight path planning [10]. Two primary factors should be considered during the path planning, i.e., UAV oblique angle and ground sample distance (GSD) [11]. Theoretically, collecting close-range thermal images with a perpendicular view to the inspected surface is recommended [12]. However, meeting these conditions during real-world UAV-enabled building inspections can be challenging since: (1) UAV needs to maintain a safe distance to the inspected façades to avoid collisions; (2) as the GSD decreases, the inspection distance decreases and the inspection duration increases significantly, posing constraints on completing the inspection within the UAV's flight time; and (3) surrounding obstacles, such as trees and power lines, may obstruct areas that would allow the UAV to achieve a perpendicular view. Therefore, it is crucial to understand the influence of different UAV inspection configurations on inspecting thermal anomalies.

Current practices have examined the influence of UAV oblique angle in thermal image-based 3D reconstruction [13] and surface temperature measurement [14], while its impact on detecting thermal anomalies stays unrevealed. Pan et al. [15] obtained similar thermal anomalies detection accuracy from images with an inspection distance of 5 m and 10 m. However, this observation was based on relatively large thermal anomalies with a dimension larger than 1.5 m. Additionally, Mayer et al. [11] investigated the influence of different UAV settings (e.g., flight speed, oblique angle and inspection distance) on the quality of the collected thermal images. However, their analysis focused only on the overall quality (e.g., image resolution, coverage, and contrast) of thermal images with a large field of view, and thus failing to provide insights in the optimal UAV configurations for close building thermal inspection and anomaly detection.

In addition to the UAV configurations, the environmental conditions also play a vital role [16]. Particularly, a minimum temperature difference of 10 ℃ between interior and exterior environments is recommended for thermal building inspection [12]. Although this temperature difference can be achieved by conducting inspections during night or early morning with heating system switched on [16], this time restraint severely impedes the widespread use of UAV-enabled building energy audits. Therefore, it is vital to explore the feasibility of identifying thermal anomalies from images collected with a relatively low difference in interior and exterior temperatures.

To better understand the influence of different factors on accurate thermal anomaly inspection, it is crucial to collect thermal images with known thermal anomalies under various conditions. However, collecting these thermal images during real-world building inspections presents challenges. To address this issue, this study designed and developed a laboratory-scale building with artificial thermal anomaly (e.g., sub-surface insulation failure and surface deterioration). Thermal images were further obtained under different UAV oblique angles, GSD, and interior and exterior temperature differences. The collected thermal images were subsequently analysed to compare the influence of different image acquisition strategies.

The structure of this paper is organised as follows: Section 2 presents the design and production of the laboratory-scale building model. Section 3 describes the laboratory experiment. Results and discussions are illustrated in Section 4. Finally, Section 5 summarises the findings with a conclusion.

2 Laboratory-scale building

To support the comparison of different image acquisition strategies for UAV-enabled building thermography, a laboratory-scale building was developed, as shown in Figure 1. Timber buildings have garnered global popularity due to their unique attributes, such as eco-friendliness, widespread availability, and relative ease of handling [17,18]. As such, a timber building was selected as the subject for this laboratory investigation. The structure decided upon was a single-panel timber-frame wall element, composed of three layers: a timber frame, a single-sided sheathing board, and thermal insulation [19,20]. This research primarily focused on thermal anomalies in an individual wall, thus the dimension and shape of the building are considered less significant and are designed in reference to [21]. A timber frame with a dimension of $600\ mm \times 600\ mm \times 600\ mm$ was first assembled, and further, the plywood panels with a thickness of $7\ mm$ were affixed to the timber frame to form the façade exterior, as demonstrated in Figure 1(a) and (b). Additionally, $25\ mm$ thick polystyrene ThermaSlab, with a thermal resistance rating of $0.66\ m^2K/W$, was applied to the façades and roof for insulation purposes.

It should be noted that conventional timber-based walls used in construction industry often incorporate a building wrap, also known as membrane, which serves primarily to weatherproof the structure by blocking rainwater while allowing for vapour transfer to mitigate condensation [22]. However, its impact on the building energy performance is minimal compared to the thermal insulation layer, particularly given that the laboratory investigation takes place indoors, absent of any rain or vapour. Therefore, to simplify the construction process, the building wrap was excluded.

Two types of thermal anomalies on building façades, i.e., surface deterioration [23] and sub-surface insulation failure [21], were added in the laboratory-scale building. Figure 1(c) shows the surface deterioration with various dimensions, achieved by accurately cutting the surface panel using a laser cutting machine. Additionally, insulation failures, such as missing and thin insulations, were achieved by manually cutting the ThermaSlab, as shown in Figure 1(d). Particularly, for the thin insulation, the thickness of the insulation was reduced to $10\ mm$. Detailed dimensions of the artificial thermal anomalies are summarised in Table 1. It should be noted that although the laboratory-building was downscaled, the anomalies were designed to mirror real-world dimensions for accurate representation.

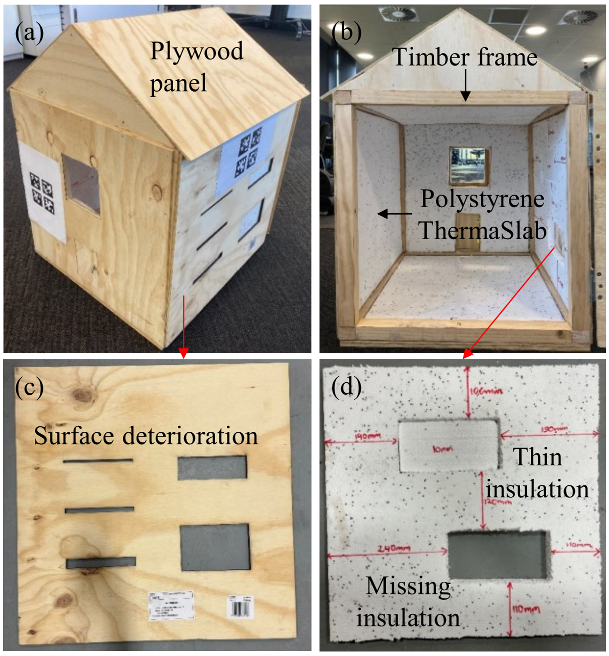

Figure 1. Laboratory-scale building with artificial anomaly: (a) exterior; (b) interior; (c) surface deterioration; (d) sub-surface insulation failure.

Table 1 Artificial thermal anomalies

Thermal anomaly	Dimension
Surface deterioration	$150\ mm \times 100\ mm$ $150\ mm \times 50\ mm$ $150\ mm \times 20\ mm$ $150\ mm \times 10\ mm$ $150\ mm \times 5\ mm$
Missing insulation	$200\ mm \times 100\ mm$
Thin insulation	$200\ mm \times 100\ mm$

3 Laboratory experiment

Laboratory experiments were further conducted using the developed building model. Figure 2(a) provides an overview of the laboratory experiment. The UAV adopted in this study is DJI Mavic 2 Enterprise Dual, equipped with a dual camera system for capturing thermal and RGB images simultaneously. The RGB camera has an image resolution of 4056×3040, and the thermal camera has a resolution of 640×480. It should be noted that the thermal camera was calibrated and registered with the RGB camera in our previous work [9].

During the experiments, a fan heater was utilised to warm up the building interior, as shown in Figure 2(b). A wireless temperature sensor was used to monitor the interior temperature. By combining with the exterior temperature (approximately 20 ℃) measured by another sensor, the temperature difference can be measured. Additionally, AprilTag [24] was attached to the building façade to calibrate the collected images and measure their corresponding GSD. The experiment mainly includes three cases, each related to a different inspection feature, i.e., interior and exterior temperature difference, GSD and UAV oblique angle.

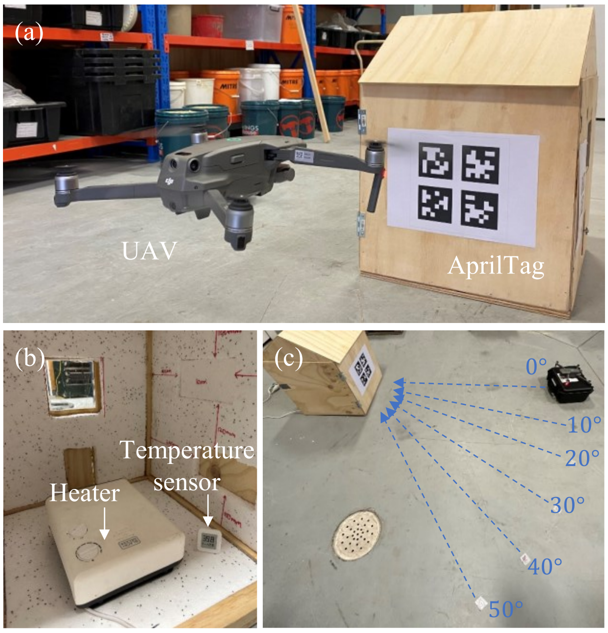

Figure 2. Laboratory experiment: (a) test overview; (b) building interior heating and temperature monitoring; (c) different UAV oblique angles.

Case 1 aimed to compare the influence of various interior and exterior temperature differences. The UAV maintained a distance of $2\ m$ (corresponding to a GSD of around $3\ mm$) and a perpendicular view to the inspected façade. Then, the heater was turned on to gradually warm up the building interior. Thermal images were collected as the temperature difference increased.

Case 2 focused on studying the influence of different GSD. After the building interior was warmed up and the temperature was stabilised, thermal images were collected with a perpendicular view to the inspected façade and at varying distances ranging from 1 m to 9 m to achieve a GSD ranging from 1.5 mm to 13 mm.

Case 3 examined the influence of different UAV oblique angles, as shown in Figure 2(c). The experiment was conducted at a distance of 2 m (corresponding to a GSD of around 3 mm) and with a stable interior and exterior temperature difference. The maximum UAV oblique angle was set at 50°, considering that thermal images collected with a larger oblique angle have a massive field of view and are rarely used for actual building inspection.

4 Results and discussion

This section demonstrates the laboratory experiment results and discusses findings regarding the image acquisition strategy for UAV-enabled building energy audit.

4.1 Temperature difference

Figure 3 shows the thermal images collected to identify insulation anomalies under different temperature differences, ranging from 1.6 ℃ to 19.5 ℃. It can be observed that the presence of missing insulation becomes noticeable at a temperature difference of 3.8 ℃, while thin insulation requires a higher temperature difference of approximately 8.1 ℃. Particularly, the colour of the thin insulation closely resembles the undamaged façade area surrounding the missing insulation, even at higher temperature difference of over 14.5 ℃. This similarity may be attributed to a small gap between the façade panel and insulation layer, allowing heat transfer from the missing insulation area to the surrounding area. This effect is particularly prominent at high temperature differences exceeding 14.5 ℃, where the missing insulation areas appear red and a small surrounding area stands out with a deep yellow colour, indicating a higher temperature. Additionally, as the temperature difference increases, the missing insulation areas becomes more distinguishable. Thus, it is recommended to capture thermal images with a higher temperature difference for identifying and quantifying missing insulation.

Thermal images collected for identifying surface deteriorations under different temperature differences are displayed in Figure 4. Surface deteriorations, even small defects, start to appear at low temperature differences, such as 3.7 ℃. As the temperature difference increases, surface deterioration becomes more noticeable. Similar to the missing insulation, the surrounding area of the surface deteriorations also exhibits a different colour compared to other undamaged façade areas. Particularly, with a significant temperature difference exceeding 11.9 ℃, surface deterioration with relatively large dimensions, such as over 20 mm, becomes distinguishable (i.e., red colour) compared to the surrounding areas (i.e., deep yellow colour). This means that a higher temperature difference allows accurately identifying and quantifying these surface deteriorations. However, smaller surface deteriorations, such as 10 mm and 5 mm defects, stay merged with the surrounding areas, making it challenging to accurately extract and segment them, even at an extremely high temperature difference of 22.6 ℃. Therefore, although small deteriorations can be visible in thermal images, accurately quantifying these deteriorations poses a challenge. Collecting thermal images with a smaller GSD may help with identifying minor anomalies, which will be discussed in the following section.

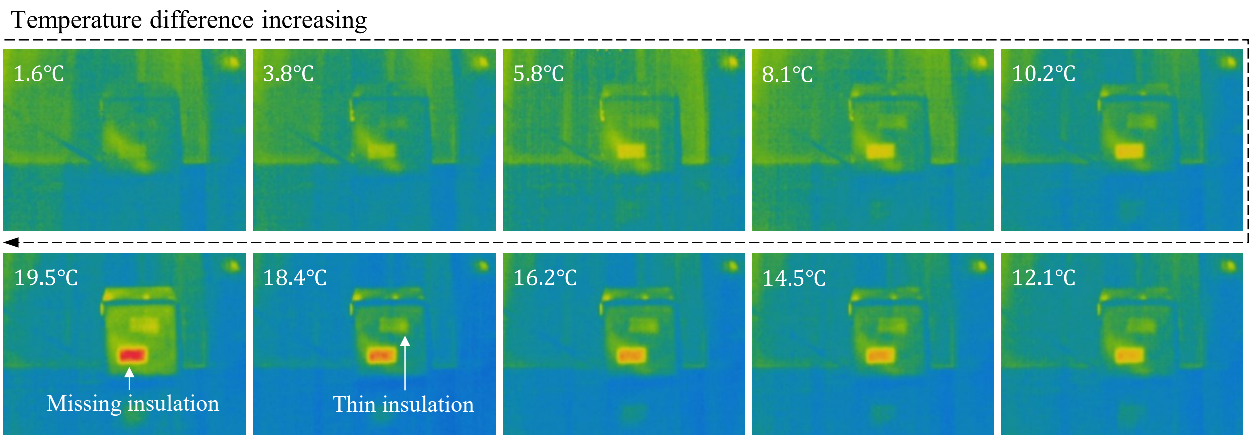

Figure 3. Thermal images of insulation anomalies under different temperature differences: GSD of around 3 mm and UAV oblique angle of approximately 0°.

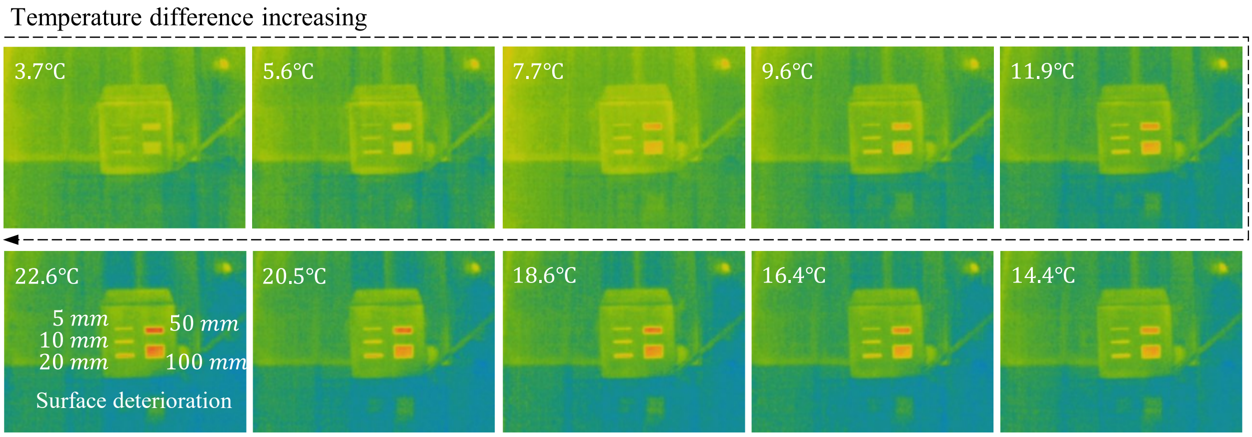

Figure 4. Thermal images of surface deterioration under different temperature differences: GSD of around 3.3 mm and UAV oblique angle of approximately 0°.

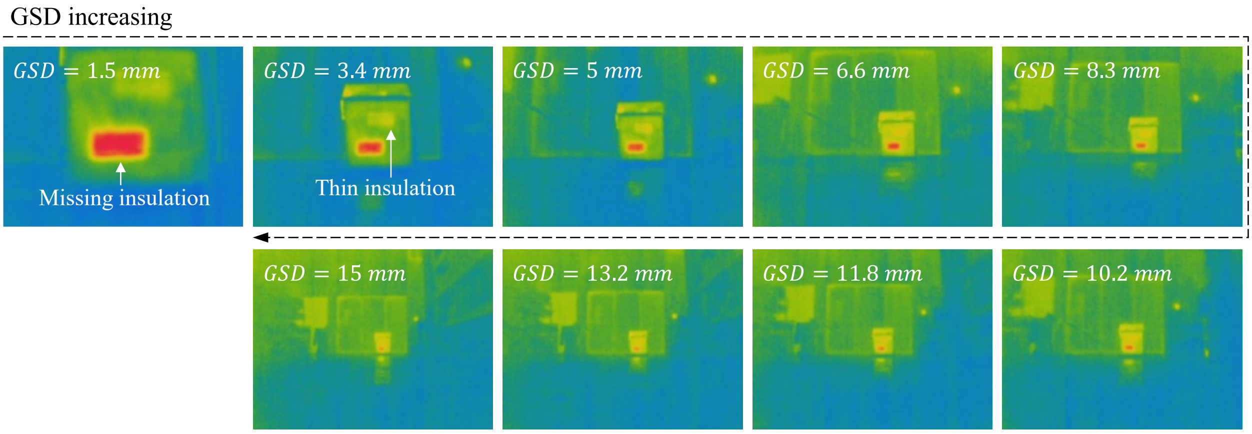

Figure 5. Thermal images of insulation anomalies under different GSD: temperature difference of around 18 °C and UAV oblique angle of approximately 0°.

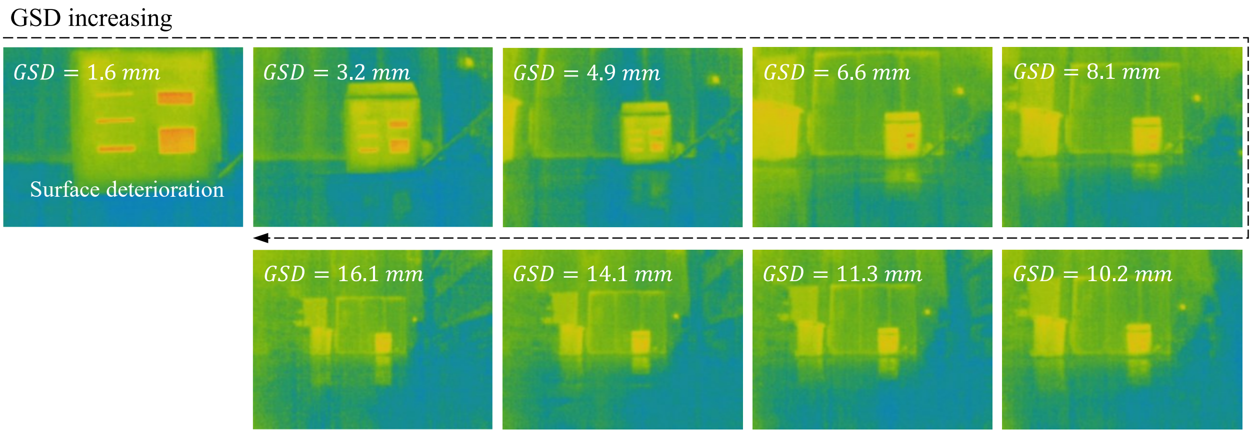

Figure 6. Thermal images of surface deterioration under different GSD: temperature difference of around 29 °C and UAV oblique angle of approximately 0°.

To summarise, an interior and exterior temperature difference exceeding 8 °C is required to detect various thermal anomalies, including minor defects, such as thin insulation. As the temperature difference increases, thermal anomalies become more noticeable in the collected UAV thermal images. Therefore, it is advisable to conduct building inspections with the highest temperature difference to achieve maximum thermal image contrast between damaged and intact areas.

4.2 GSD

To understand the influence of GSD in the UAV-enabled building thermography, thermal images were collected with a GSD ranging from 1.5 mm to 16 mm, as shown in Figure 5 and Figure 6. The missing insulation remains visible as a distinct red colour, even with a GSD of 1.5 mm, as shown in Figure 5. However, the thin insulation starts to blend with the undamaged areas when the GSD reaches 6.6 mm. Similarly, small surface deteriorations of 5 mm, 10 mm and 20 mm become invisible with a GSD of 6.6 mm. Additionally, even large surface deteriorations of 50 mm and 100 mm disappeared from the thermal image taken with a GSD of 10.2 mm. This may be due to the thin insulation and surface deteriorations exhibiting a smaller temperature difference compared to the undamaged areas, as they are relatively minor thermal damages compared to the missing insulation. Based on these observations, a GSD of within 5 mm is recommended to ensure that all thermal damages are visible in the collected thermal images.

However, a smaller GSD may be needed to accurately measure and quantify these thermal damages, especially with regard to minor thermal anomalies. For example, surface deterioration with a width of 10 mm is distinguishable as red colour in the thermal image collected with a GSD of 1.6 mm, while starting merged with the surrounding areas (appearing as deep yellow colour) with a GSD of 3.2 mm, as shown in Figure 6.

Therefore, a multi-scale thermal image collection strategy is recommended considering the limited flight time of most UAV (around 30 mins). Specifically, thermal images may first be collected with a GSD less than 5 mm distance to identify all possible areas with thermal damages on building façades. Then, close-range thermal images with a smaller GSD should be taken around these identified areas to ensure accurate detection and measurement of the thermal damages. Considering that most commercial UAV can not fly too close to the inspected surface due to safety concerns, it is recommended to develop customised UAV (e.g., wall-climbing UAV [25]), that are specifically designed for collecting close-range images.

4.3 UAV oblique angle

Figure 7 and Figure 8 display thermal images collected from various UAV oblique angles, ranging from 0° to 50°. Although thermal anomalies stay visible in the thermal images, even with a large oblique angle of 50°, the contrast between the damaged and the undamaged façade areas decreases as the oblique angle increases. Particularly, when the oblique angle reaches 30°, the missing insulation starts to blend with the surrounding areas, as shown in Figure 7. This could be attributed to the fact that a large oblique angle may capture reflections from other sources, thereby reducing the ability to accurately capture the emissivity of the target surfaces [14]. Additionally, as the UAV oblique angle increases, the field of view of the thermal images also increases significantly, covering unwanted backgrounds. These backgrounds can also reduce the image contrast of the target areas. Therefore, a UAV oblique angle within 30° is recommended when collecting thermal images for building energy audits.

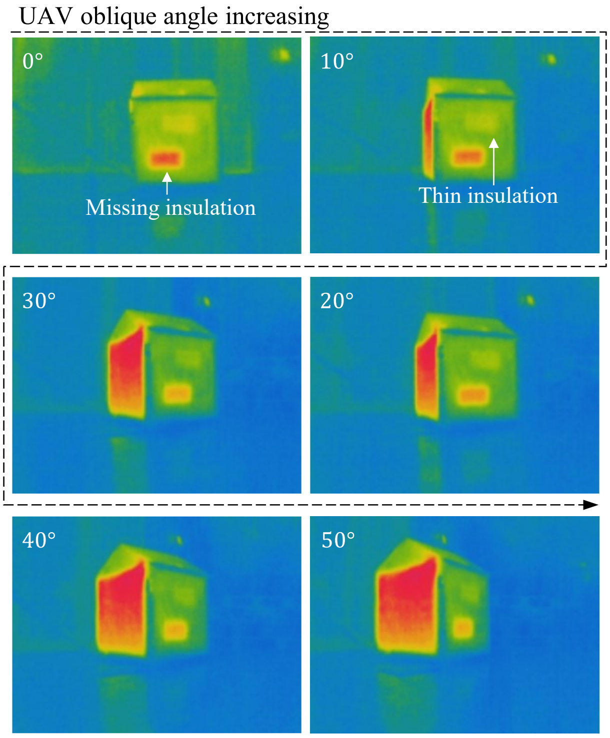

Figure 7. Thermal images of insulation anomalies under different UAV oblique angles: temperature difference of around 16 ℃ and GSD of approximately 3.3 mm.

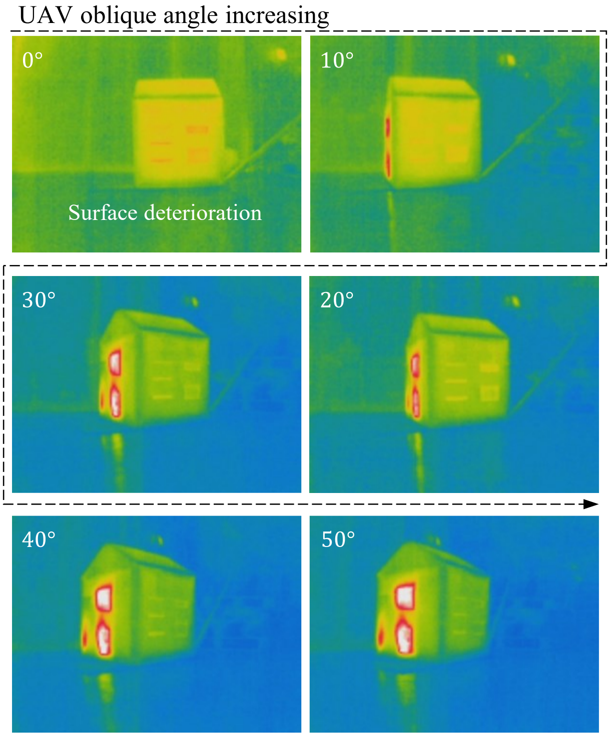

Figure 8. Thermal images of surface deterioration under different UAV oblique angles: temperature difference of around 28 ℃ and GSD of approximately 3.3 mm.

5 Conclusion

This paper compared three features of image acquisition strategies of UAV thermography for building energy audit. A laboratory-scale building with artificial thermal anomalies, such as sub-surface insulation failure and surface deterioration, was first developed. Furthermore, thermal inspections were conducted under various conditions, such as different UAV oblique angles, GSD, and interior and exterior temperature differences. The results indicate that:

(1) An interior and exterior temperature difference exceeding 8 ℃ is necessary to identify potential thermal anomalies from UAV thermal images. Conducting building inspections with the highest temperature difference is advisable to achieve maximum thermal image contrast between damaged and intact areas.

(2) A GSD of within 5 mm, is required to ensure the visibility of thermal anomalies in the collected thermal images. A multi-scale thermal image collection strategy is recommended to ensure efficient and accurate measurement of various thermal anomalies, especially minor defects.

(3) An UAV oblique angle of within 30° is recommended to be maintained during the thermal building inspection.

The comparison presented in this paper has some limitations and room for improvement. As an ongoing research project, future work will involve quantitatively evaluating thermal damage detection from the collected thermal images and investigating the interferences between the three features. Additionally, given the relatively straightforward nature of the constructed laboratory-scale building, forthcoming investigations will involve field studies on real-world buildings, which may contain more complex anomalies, to validate the identified image acquisition strategies.

Acknowledgements

The authors appreciate the assistance provided by two undergraduate students, Yuvraj Behal and Mohammed Samdani of the University of Auckland, in the development of the laboratory-scale building.

References

[1] C. Delmastro, O. Chen, Buildings. The International Energy Agency (IEA) (2023). Retrieved 28 February 2024 from https://www.iea.org/reports/buildings.

[2] M.H. Shariq, B.R. Hughes, Revolutionising building inspection techniques to meet large-scale energy demands: A review of the state-of-the-art, Renewable and Sustainable Energy Reviews 130 (2020), pp. 109979, https://doi.org/10.1016/j.rser.2020.109979.

[3] M. Martin, A. Chong, F. Biljecki, C. Miller, Infrared thermography in the built environment: A multi-scale review, Renewable and Sustainable Energy Reviews 165 (2022), pp. 112540, https://doi.org/10.1016/j.rser.2022.112540.

[4] A. Kirimtat, O. Krejcar, A review of infrared thermography for the investigation of building envelopes: Advances and prospects, Energy and Buildings 176 (2018), pp. 390-406, https://doi.org/10.1016/j.enbuild.2018.07.052.

[5] A. Ramón, A. Adán, F. Javier Castilla, Thermal point clouds of buildings: A review, Energy and Buildings 274 (2022), pp. 112425, https://doi.org/10.1016/j.enbuild.2022.112425.

[6] T. Rakha, A. Gorodetsky, Review of Unmanned Aerial System (UAS) applications in the built environment: Towards automated building inspection procedures using drones, Automation in Construction 93 (2018), pp. 252-264, https://doi.org/10.1016/j.autcon.2018.05.002.

[7] N. Bayomi, S. Nagpal, T. Rakha, J.E. Fernandez, Building envelope modeling calibration using aerial thermography, Energy and Buildings 233 (2021), pp. 110648, https://doi.org/10.1016/j.enbuild.2020.110648.

[8] Z. Mayer, J. Kahn, Y. Hou, M. Götz, R. Volk, F. Schultmann, Deep learning approaches to building rooftop thermal bridge detection from aerial images, Automation in Construction 146 (2023), pp. 104690, https://doi.org/10.1016/j.autcon.2022.104690.

[9] C. Zhang, Y. Zou, J. Dimyadi, R. Chang, Thermal-textured BIM Generation for Building Energy Audit with UAV Image Fusion and Histogram-based Enhancement, Energy and Buildings 301 (2023), pp. 113710, https://doi.org/10.1016/j.enbuild.2023.113710.

[10] M. Mahmoodzadeh, V. Gretka, P. Mukhopadhyaya, Challenges and opportunities in quantitative aerial thermography of building envelopes, Journal of Building Engineering 69 (2023), pp. 106214, https://doi.org/10.1016/j.jobe.2023.106214.

[11] Z. Mayer, A. Epperlein, E. Vollmer, R. Volk, F. Schultmann, Investigating the Quality of UAV-Based Images for the Thermographic Analysis of Buildings, Remote Sensing 15 (2) (2023), pp. 301, https://doi.org/10.3390/rs15020301.

[12] International Organization for Standardization (ISO), Thermal insulation-Qualitative detection of thermal irregularities in building envelopes-Infrared method, Standard ISO 6781, 1983, https://www.iso.org/standard/13277.html.

[13] S. Dabetwar, N.N. Kulkarni, M. Angelosanti, C. Niezrecki, A. Sabato, Sensitivity analysis of unmanned aerial vehicle-borne 3D point cloud reconstruction from infrared images, Journal of Building Engineering 58 (2022), pp. 105070, https://doi.org/10.1016/j.jobe.2022.105070.

[14] J. Ortiz-Sanz, M. Gil-Docampo, M. Arza-García, I. Cañas-Guerrero, IR thermography from UAVs to monitor thermal anomalies in the envelopes of traditional wine cellars: Field test, Remote Sensing 11 (12) (2019), pp. 1424, https://doi.org/10.3390/rs11121424.

[15] N.H. Pan, C.H. Tsai, K.Y. Chen, J. Sung, Enhancement of external wall decoration material for the building in safety inspection method, Journal of Civil Engineering and Management 26 (3) (2020), pp. 216-226, https://doi.org/10.3846/jcem.2020.11925.

[16] E. Lucchi, Applications of the infrared thermography in the energy audit of buildings: A review, Renewable and Sustainable Energy Reviews 82 (2018), pp. 3077-3090, https://doi.org/10.1016/j.rser.2017.10.031.

[17] Z. Chen, M. Popovski, C. Ni, A novel floor-isolated re-centering system for prefabricated modular mass timber construction – Concept development and preliminary evaluation, Engineering Structures 222 (2020), pp. 111168, https://doi.org/10.1016/j.engstruct.2020.111168.

[18] M. Caniato, A. Marzi, S. Monteiro da Silva, A. Gasparella, A review of the thermal and acoustic properties of materials for timber building construction, Journal of Building Engineering 43 (2021), pp. 103066, https://doi.org/10.1016/j.jobe.2021.103066.

[19] V.Ž. Leskovar, M. Premrov, Influence of glazing size on energy efficiency of timber-frame buildings, Construction and Building Materials 30 (2012), pp. 92-99, https://doi.org/10.1016/j.conbuildmat.2011.11.020.

[20] K. Vogrinec, M. Premrov, E. Kozem Šilih, Simplified modelling of timber-framed walls under lateral loads, Engineering Structures 111 (2016), pp. 275-284, https://doi.org/10.1016/j.engstruct.2015.12.029.

[21] M. Puliti, G. Montaggioli, A. Sabato, Automated subsurface defects' detection using point cloud reconstruction from infrared images, Automation in Construction 129 (2021), pp. 103829, https://doi.org/10.1016/j.autcon.2021.103829.

[22] K. Orlowski, Automated manufacturing for timber-based panelised wall systems, Automation in Construction 109 (2020), pp. 102988, https://doi.org/10.1016/j.autcon.2019.102988.

[23] E. Bauer, E. Pavón, E. Barreira, E. Kraus De Castro, Analysis of building facade defects using infrared thermography: Laboratory studies, Journal of Building Engineering 6 (2016), pp. 93-104, https://doi.org/10.1016/j.jobe.2016.02.012.

[24] E. Olson, AprilTag: A robust and flexible visual fiducial system, 2011 IEEE International Conference on Robotics and Automation, 2011, pp. 3400-3407, https://doi.org/10.1109/ICRA.2011.5979561.

[25] S. Jiang, J. Zhang, Real-time crack assessment using deep neural networks with wall-climbing unmanned aerial system, Computer-Aided Civil and Infrastructure Engineering 35 (6) (2020), pp. 549-564, https://doi.org/10.1111/mice.12519.